The influence of various solvents extraction on chemical properties on Chang 7 shale, Ordos Basin, China

Yan Cao[1,2], Zhijun Jin[1,2], Rukai Zhu[1,2,3], Kouqi Liu[1,2]

[1]Institute of Energy, Peking University, Beijing, 100871, China
[2]School of Earth and Space Sciences, Peking University, Beijing, 100871, China
[3]Research Institute of Petroleum Exploration & Development, PetroChina, Beijing, 100083, China

Correspondence to: Zhijun Jin (jinzj1957@pku.edu.cn)

Abstract. To explore the effect of various solvents extraction on the chemical property of shales, several lacustrine shales from Chang 7 member of the Upper Triassic Yanchang Formation, Ordos Basin with maturities from marginally mature (T_{max}=439℃) to late mature (T_{max}=456℃) were extracted by using acetone, tetrahydrofuran (THF), carbon disulfide (CS_2), and benzene, respectively. Fourier transform infrared spectroscopy (FTIR) was employed to examine the functional groups of the samples before and after extraction with different solvents. The results showed that the extraction yield from shale with THF is significantly higher than that of other solvents, which may be related to the properties of the THF, including the aromatic structure, high boiling point, excellent Hansen solubility parameters, and strong polarity. The total organic carbon (TOC)-normalized yield of the mature sample J1 is significantly higher than that of other samples, which may be related to that the J1 sample is at the peak of hydrocarbon generation, thus a large number of kerogens were cracked into oil and bitumen. The aromaticity of organic matter (OM) increases with the increase of maturity. The length of the aliphatic chains of the OM first increased with the increase of maturity before late maturity stage, and then decreased in late maturity stage. The extraction of shales with solvents hardly changes the length of aliphatic chains. Higher aromaticity is observed in shale residues after THF extractions than other solvents (i.e., acetone, CS_2, benzene).

1 Introduction

Due to the increasingly serious energy shortage problems associated with the exhaustion of fuel energy resources, potential unconventional fossil sources are highly desired (Yang et al., 2019; Li et al., 2022). The quest to product unconventional petroleum-based fuels and achieve energy independence is being aggressively pursued in China and the United States (Overland, 2015). In the past few years, shale oil has been regarded as an important resource that can be exploited commercially due to the technical innovations of three-dimensional development in horizontal wells and fracture-controlled fracturing (Li et al., 2019; Zhou et al., 2020a; Lei et al., 2021; Yang et al., 2021a). For China, the government has been encouraging shale oil developments to address the shortage of domestic oil resources, and the rising energy demand and to safeguard the country's long-term energy security (Yang et al., 2019; Hu et al., 2020; Zhou et al., 2020b; Lu et al., 2022).

Extraction has become a common shale pretreatment method in the laboratory to study the pore structures related to OM (Qi et al., 2019; Wang et al., 2020; Yang et al., 2021b). However, different solvents could affect shale extraction efficiency and methane adsorption capacity (Cao et al., 2019, 2020). For the shale samples, the extraction by using acetone, CS_2, and benzene can be used to reveal the micropores, mesopores, and macropores, respectively (Cao et al., 2019). In addition, during the development of shale oil, the chemical properties of shale after being extracted by using different organic solvents are also different (Cao et al., 2020). Wei et al. (2014) found that the hydrocarbons in toluene extract exhibit remarkable aromaticity. Furmann et al. (2013) showed that the organic aromaticity of extractions from dichloromethane is greater than that from methanol.

A large number of studies focus on either the changes in shale pore structure before and after extraction (Gorynski et al., 2019; Qi et al., 2019; Yang et al., 2021a,b) or the functional groups of OM extracted from underground fossil energy (Chen et al., 2012; Mastalerz et al., 2012; Furmann et al., 2013; Wei et al., 2014). In fact, underground shale is often washed out of OM by organic solvent extraction in the laboratory to explore the relationship between OM and inorganic mineral skeleton in shale. It is worth mentioning that this study is a continuation of our earlier published study, which details the findings about influence of extraction on shale pore structure with different maturity using various solvents (Cao et al., 2019, 2020). However, the study of the changes in chemical properties in lacustrine organic-rich shale of different maturity before and after extraction with different solvents is rarely reported. Our results of the study will help in the selection of organic solvents for oil-washing experiments in shales of different maturity.

Fourier Transform Infrared Spectroscopy (FTIR) is an advanced method for the determination of chemical structures (e.g., functional groups) of OM (Wei et al., 2014). In this study, several lacustrine shales with different maturities from Chang 7 member of the Upper Triassic Yanchang Formation, Ordos Basin, central China were collected. The present study is a continuation of our previous research (Cao et al., 2019, 2020), soxhlet extractions with four different solvents (tetrahydrofuran, carbon disulfide, benzene, and acetone) were performed on the selected shale samples. Interestingly, the Fourier Transform Infrared Spectroscopy (FTIR) was performed on the samples before and after the extraction. After that, the influence of various solvent extraction on chemical properties in lacustrine shale of different maturity was summarized.

1 Geological settings and samples

According to the basement and faults, the Ordos Basin is divided into six secondary structural units, namely the Weibei uplift, the Yishan slope, the Tianhuan depression, the Yimeng uplift, the western margin thrust belt, and Jinxi flexural fold belt (Fig. 1) (Guo et al., 2014). The Yishan slope is inclined to the west with a slope of about 1° (Guo et al., 2014). The Chang 7 member was developed during the largest lacustrine flooding in the lake basin (Fig. 1) (Guo et al., 2014). Yellowish tuff intervals are interbedded within the Yanchang sediments ranging from 0.2 to 0.45 cm (0.08–0.18 in.) (Qiu et al., 2014). The Yanchang Formation of the upper Triassic can be divided into 10 sub-segments (i.e., Chang 1-10) (Fig. 2). The Chang 7 member is mainly made up of silty mudstone and shales and has great potential for shale oil/gas (Fig. 2) (Duan et al., 2008;

Lei et al., 2015). The Chang 7 member shale develops a large area of high-quality source rocks (about 5×10^4 km^2), which is rich in oil-prone OM derived from acritarchs (Leiosphaeridia species) as well as some Botryococcus (Ji et al., 2010). The cumulative thickness is mostly between 10 m and 50 m, and the maximum thickness can reach more than 80 m (Guo et al., 2014). In this paper, several shale samples with different maturities in Chang 7 member of the Upper Triassic Yanchang Formation were obtained from wells Huan 317, Jian 1, Luohe 10, and Jinghe 2, respectively (Fig. 1). The samples selected for this study have been analyzed in our previous publications (Cao et al., 2020).

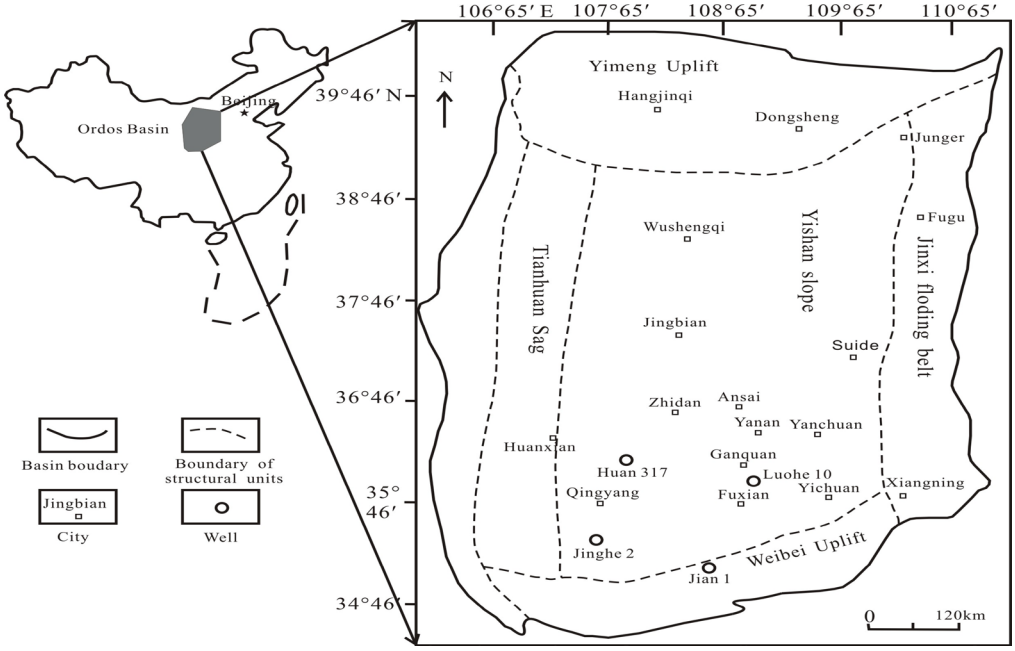

Fig. 1. Locations of sampling wells and simplified structural framework across the Ordos Basin (modified from Cao et al. 2019).

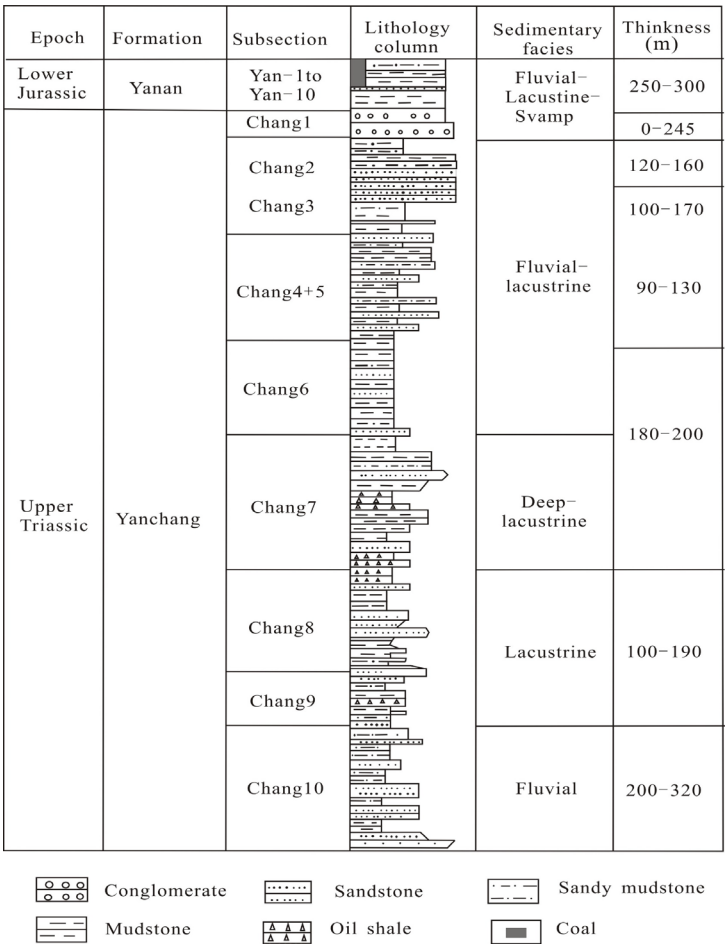

Fig. 2. The strata and sedimentary characteristics of the Yanchang Formation of the Upper Triassic (modified from Cao et al. 2020).

3 Experiments

3.1 Geochemical analysis

The samples were crushed to 180-200 mesh prior to geochemical analysis. The TOC content was tested by a Leco C/S-344 Carbon/Sulfur analyzer. The type, maturity, and hydrocarbon generation potential of OM were determined. The temperature at which the most S_2 is generated is regarded as the maximum pyrolysis yield temperature (T_{max}, °C) and the hydrogen index (HI, mg HC/g TOC) was obtained from the ratio of S_2 to TOC (Peters, 1986).

3.2 X-ray diffraction

The samples were tested by a D/max-2500 diffractometer, and the tests follow two separate processes of the CPSC procedure (China Petroleum Standardization Committee, 2010). The actual mineral content of the samples was obtained by quantitative X-ray diffraction (XRD) analysis of samples smaller than 200 mesh (<0.075 mm).

3.3 Soxhlet extraction

The bulk shale samples were uniformly crushed into 60 mesh with a laboratory knife mill and then evenly divided into five parts. The sample was extracted using solvents of different aromaticity, polarity, and permeability, namely acetone, tetrahydrofuran, carbon disulfide, and benzene, and the remaining original sample was used as a control. About 1000g solvent and 50g shale sample were sealed in a Soxhlet extractor to prevent solvent loss. The extraction time lasted 150h until the solvent is colourless. Samples were named according to their corresponding abbreviated well names (JH2, J1, LH10, and H317) (Table 2), and the original shale samples were marked by the shorthand subscript following the sample name ($JH2_{orig}$, $J1_{orig}$, $LH10_{orig}$, and $H317_{orig}$). The residue (e.g., JH2) from THF, acetone, CS_2, and benzene extraction was clearly characterized by $JH2_T$, $JH2_A$, $JH2_C$, and $JH2_B$, respectively.

3.4 Potassium bromide (KBr)-FTIR analysis

Both powdered original shale samples and their corresponding extracted shale residues (~2mg) were blended with potassium bromide (KBr, ~200mg) and pressed into pellets. Through the use of a Nicolet 6700 FT-IR spectrometer collecting 200 scans per sample at a resolution of 4 cm^{-1}, the vibration frequencies of specific atomic bonds were analyzed. Thus, the chemical functional groups could be assessed using a standard semi-quantitative technique. For KBr-FTIR characterization, each spectrum was recorded in the spectral range of 400-3250 cm^{-1}. The bands of absorption were identified by comparing the spectrums with published studies (Drobniak and Mastalerz, 2006; Furmann et al., 2013).

According to a manual mode, the band area was determined using the ORIGIN software. These integrated band areas were used to calculate ratios for (1) aromaticity: AR1=[(δ Ar C = C/ν Al C-H) + δ Ar C=C], AR2=(ν Ar C-H/ν Al C-H), AR3=(γ Ar C-H/ν Al C-H); (2) length of aliphatic chains: LAC= (CH_2/CH_3) in ν Al C-H and (3) degree of substitution (DOS) of aromatic sites by alkyl groups: DOS= (γ Ar C-H (1 adjacent H)/γ Ar C-H (4 adjacent H)) (Wei et al., 2014). The detailed definitions of the parameters can be found in Tables 1 and 4.

The representative spectrums of the original shales and corresponding residues are presented in Fig. 5 and Fig. 6, respectively. In terms of the length of aliphatic chains (LAC), longer n-alkyl chains are determined by CH_2 bands, whereas shorter n-alkyl and branched aliphatic chains are indicated by CH_3 bands (Table 4). The DOS of aromatic rings represents the fraction of aromatic sites where hydrogen atoms are substituted by alkyl groups (Table 4).

Table 1. Fourier Transform Infrared (FTIR) bands used in this study (Chen et al., 2012).

FTIR band	For marginally mature shales JH2 T_{max} (439°C)	For mature shales J1 T_{max} (449°C)	For late mature shale LH10 T_{max} (454°C)	For late mature shale H317 T_{max} (456°C)
	Wave numbers (cm^{-1})	Wave numbers (cm^{-1})	Wave numbers (cm^{-1})	Wave numbers (cm^{-1})
ν Ar C-H	3046-2992	3062-2992	3084-3005	3062-3000
ν Al C-H	2970-2812	2970-2809	2983-2809	2984-2814
ν_{as} CH_3	2970-2874	2970-2877	2970-2887	2984-2882
ν_s CH_2	2874-2812	2877-2809	2887-2798	2882-2814
δ Ar C=C	1705-1575	1701-1561	1719-1552	1707-1552
δ Al C-H	1484-1386	1477-1400	1487-1389	1482-1381
γ Ar C-H	945-667	946-673	939-673	948-673
γ Ar C-H 1	945-833	930-886	940-812	948-817
γ Ar C-H 2	833-721	814-707	812-709	817-707
γ Ar C-H 4	721-667	707-673	709-673	707-673

Ar–aromatic; Al–aliphatic; ν–stretching vibration; δ–deformation vibration in plane; γ–deformation vibration out of plane; as–asymmetric; s–symmetric.

4 Results

4.1 Geochemical characteristics

The geochemical features of shales were listed in Table 2. Four selected samples span from marginally mature (JH2, 439°C) to Late mature (H317, 460°C) based on the Chinese continental hydrocarbon source rock geochemical evaluation method (SY/T 5735-1995). The kerogen type of selected samples is type I or II_1 (Fig. 3) (Tong et al., 2011). TOC content is generally high, ranging from 3.79 to 22.19 wt.% (Table 2). The hydrocarbon generation potential (S_1+S_2) ranges from 8.11 mg/g to 127.42 mg/g. Table 2 shows that the hydrogen index (HI) of the samples is in the range of 155 mg/g~528 mg/g.

Table 2. Geochemical features of the original shale samples and the corresponding residues.

Sample	S_1(mg/g)	S_2(mg/g)	T_{max} (°C)	TOC (%)	OM type	HI (mg/g)	Maturity stage
JH2	10.19	117.23	439	22.19	I	528	Marginally mature
J1	2.23	5.88	449	3.79	II_1	155	Mature
LH10	11.31	47.42	454	16.23	I	292	Late mature
H317	5.39	33.89	456	18.03	I	188	Late mature

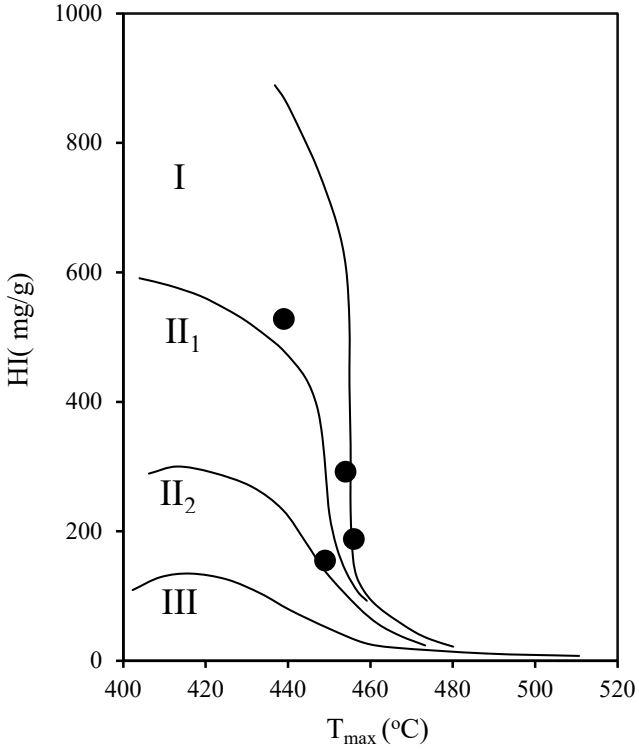

Fig. 3. Plot of HI versus T_{max} for the original shales (based on Espitalie et al. 1985)

4.2 Mineral compositions

125 The samples contain a large amount of clay minerals (42.8 wt. %-54.2 wt. % with an average of 48.15%). Illite/smectite mixed-layer or Illite are the most dominant clay types (Table 3). In general, the content of the felsic component is between 19.5 wt. %-52.2 wt. % with the average of 40.63%. In addition, the pyrite content of the studied samples varies greatly, ranging from 0.9 to 25.5 wt.% (Table 3).

Table 3. Mineral compositions of the studied samples.

Sample	Quartz (wt. %)	Feldspar (wt. %)	Pyrite (wt. %)	Gypsum (wt. %)	All clays (wt. %)	Illite/Smectite (wt. %)	Illite (wt. %)	Kaolinite (wt. %)	Chlorite (wt. %)	Mixed-layer ratio (I/S) S, %
JH2	12	7.5	25.5	0.8	54.2	70	9	21	/	19
J1	36.5	12.7	0.9	/	49.9	62	18	8	12	18
LH10	23.2	29	2.1	/	45.7	66	15	7	12	11
H317	29.7	11.9	15.6	/	42.8	2	88	2	8	24

/, the content of individual mineral was not determined.

4.3 Extraction yields

The extraction data of the studied samples with different solvents is shown in Fig. 4. Among all the solvents, THF has the highest extraction efficiency (2.44 wt. %-4.43 wt. %) (Fig. 4a). According to the TOC-normalized yield of extracts, the mature samples J1 (T_{max} 449℃) had significantly higher extractable (13.48 wt. %-56.91 wt. %) than other samples (⩽5.28 wt. %) (Fig. 4b).

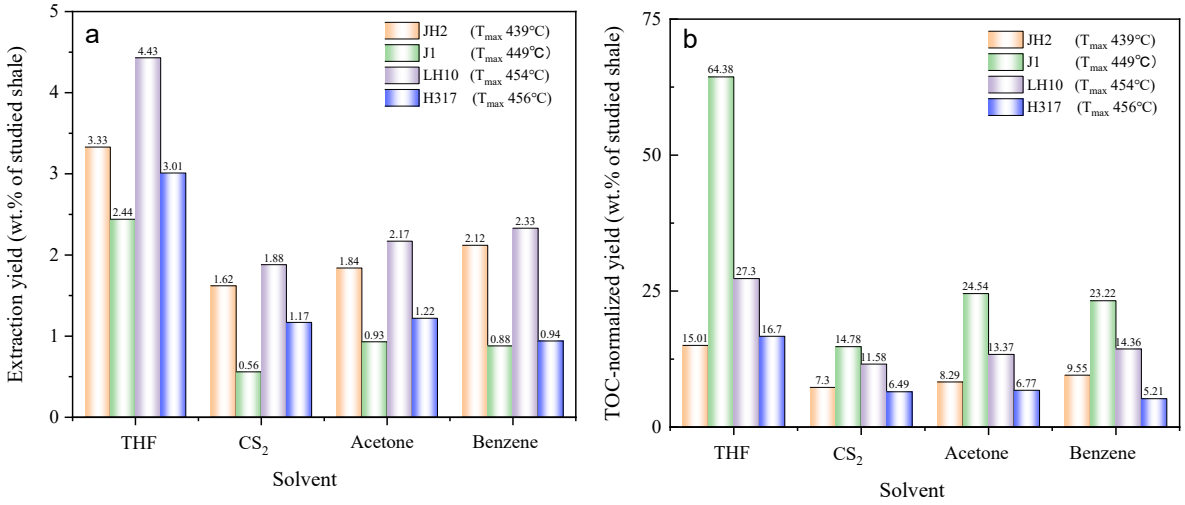

Fig. 4. Extraction data of the studied samples with solvents of acetone, THF, benzene, and CS_2 (a. original extraction yield b. TOC-normalized yield of extracts).

4.4 FTIR spectroscopy

The representative spectrums of the original shales and corresponding residues are presented in Fig. 5 and Fig. 6, respectively. The FTIR results after extraction are summarized in Table 4. The OM in shale is a three-dimensional macromolecule composed of aromatic clusters and aliphatic chains (Tong et al., 2011; Guan et al., 2015; Wang et al., 2016; Wang et al., 2017; Zhao et al., 2018). The aromaticity (i.e., AR2 and AR3) of the samples follows the order: H317 (3.327) > LH10 (3.225) > J1 (3.038) > JH2 (2.828) (Table 4), which are consistent with maturity. In addition, shale residues from THF extraction possess higher aromaticity than those from other solvents. Unlike aromaticity, the length of aliphatic chains (LAC) doesn't increase monotonically with the increase of maturity (Table 4). However, there is no regularity in the DOS (i.e., the fraction of aromatic sites where hydrogen atoms are substituted by alkyl groups) of different maturity shales, and the DOS of shale before and after extraction with different solvents demonstrated an irregular change (Table 4).

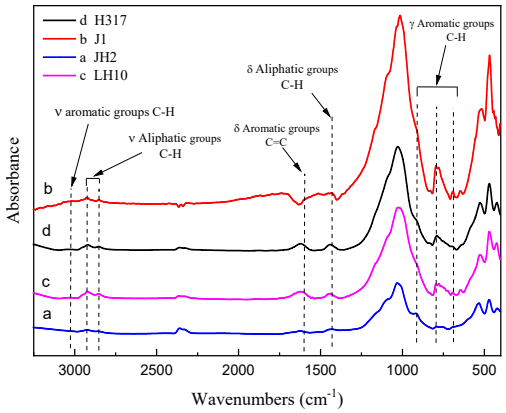

Fig. 5. FTIR spectra of original (a) marginally mature sample $JH2_{orig}$ (T_{max}=439°C) (b) the mature sample $J1_{orig}$ (T_{max}=449°C) (c) late mature sample $LH10_{orig}$ (T_{max}=454°C) and (d) late mature sample $H317_{orig}$ (T_{max}=456°C).

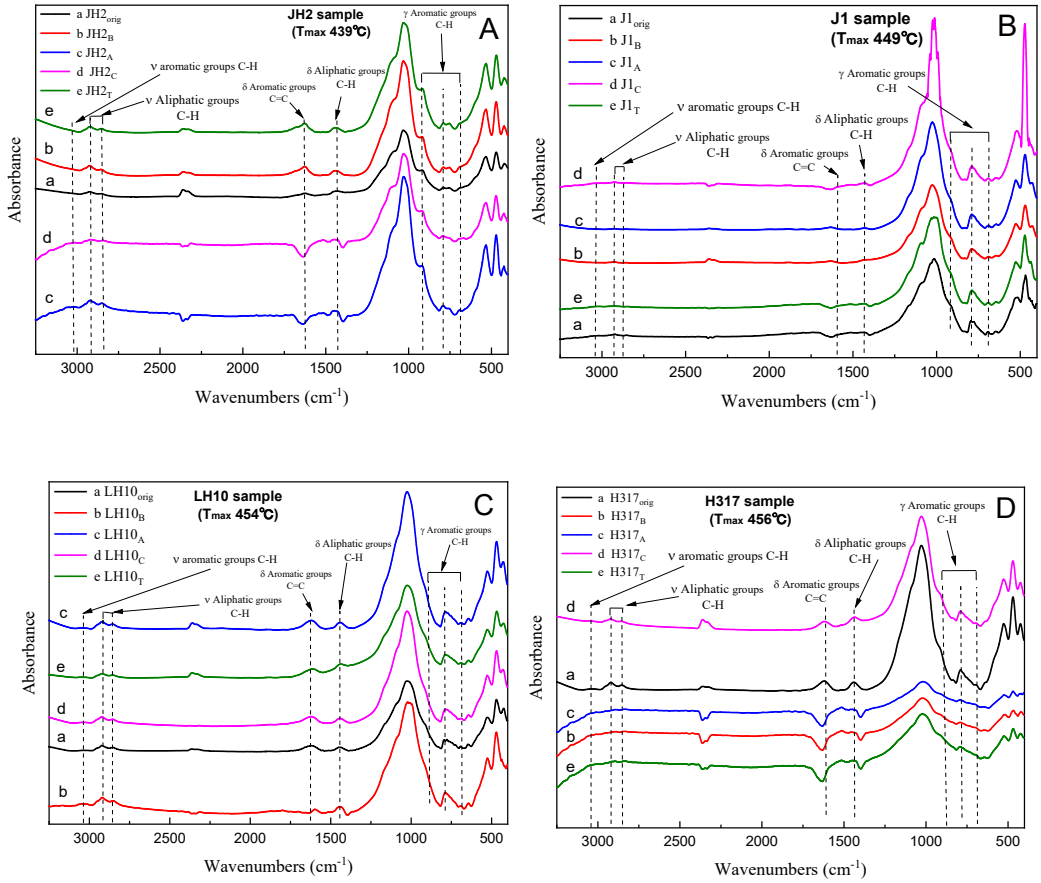

Fig. 6. A comparison of FTIR spectra of original samples and residues.

Table 4. FTIR results from original shales and extracted shale residues.

	FTIR absorbance ratios*				
	AR1[#]	AR2	AR3	LAC	DOS
Shale residues after extraction:					
JH2 shale:					
Original shale	2.352	0.010	2.818	0.242	11.498
After extraction with:					
acetone	0.000	0.039	2.156	0.288	8.935
CS_2	0.000	0.092	2.449	0.269	6.861
benzene	4.996	0.004	2.412	0.252	9.382
THF	5.114	0.024	2.893	0.262	10.494
J1 shale:					
Original shale	6.399	0.064	2.974	0.257	1.700
After extraction with:					
acetone	6.731	0.011	20.006	0.232	1.654
CS_2	9.573	0.172	16.903	0.308	1.997
benzene	5.063	0.012	18.416	0.237	2.012
THF	0.000	0.253	22.122	0.335	1.492
LH10 shale:					
Original shale	7.167	0.103	3.122	0.298	2.897
After extraction with:					
acetone	10.632	0.101	3.500	0.270	2.655
CS_2	8.381	0.092	3.371	0.268	2.933
benzene	2.466	0.228	3.000	0.352	2.859
THF	7.667	0.119	4.041	0.289	2.780
H317 shale					
Original shale	8.347	0.068	3.259	0.272	1.686
After extraction with:					
acetone	0.000	0.627	2.844	0.858	2.181
CS_2	5.472	0.066	3.749	0.243	2.129
benzene	0.000	0.268	2.313	0.485	2.031
THF	0.000	0.3420	3.753	0.551	1.624

155 The integrated peak areas were used to calculate FTIR ratios.

AR1=0 for residues because aromatic bands (δ Ar C=C, ν Ar C-H) were not present in the FTIR spectrum.

5 Discussions

5.1 The influence of solvents on extraction yield and composition of the soluble mixture

Previous studies have found that the extraction yields of shale and the composition of the soluble mixture are related to the properties of the solvent, extraction temperature, the geochemical parameters of the shale, and so on (Hu et al., 1999; Olukcu et al., 1999; Shaohui et al., 2000; Abourriche et al., 2013; Cao et al., 2019). As the polarity of the solvent increases, the extraction yield increases accordingly (Masaki et al., 2004). The solvent dissolution capacity has obvious temperature dependence, and the dissolution capacity increases with the increase of temperature (Hu et al., 1999). The increase in extraction pressure and temperature will promote the activation energy of the sample (Allawzi et al., 2011).

The Hansen solubility parameters of the four solvents are shown in Table 5, the extraction ability of CS_2 is similar to that of benzene (Table 5). Because of the aromatic structure, high boiling point, and strong polarity, THF could have a stronger extraction ability than other solvents (Table 5).

Table 5. The properties of the four solvents (Cao et al., 2020)

Solvent	Hansen solubility parameters			Polarity	Boiling point	Aromaticity
	Dispersion	Polarity	H-bond			
THF	16.8	5.7	8	4.2	65 °C	Aromatic
CS_2	20.2	0	0.6	0.15	46.5 °C	Non-aromatic
Acetone	15.5	10.4	7	5.4	56 °C	Non-aromatic
Benzene	18.4	0	2	3	80 °C	Aromatic

Allawzi et al. (2011) found that the OM obtained by solvent extraction is mainly composed of low molecular weight compounds (e.g., saturated hydrocarbons, olefin hydrogen, aromatic compounds). Our results show that the extraction yield of shale with THF is significantly higher than that of other solvents (Fig. 4a), which could be attributed to that a mass of the heaviest macromolecular compound-asphaltene was screened out (Cao et al., 2020). The significant elimination of OM (i.e., asphaltene) by THF may be related to the properties of the THF, including the aromatic structure (Johnson et al., 1967), high boiling point (Cao et al., 2019), excellent Hansen solubility parameters and strong polarity (Toolan et al., 2016) (Table 5), which could assist to destroy the interact between shale matrix and the asphaltenes (i.e., a complex molecular architecture with a central polycyclic aromatic hydrocarbon (PAH) with peripheral alkane substituents) (Schuler et al., 2017) of PAH molecular polymerization (Schuler et al., 2015).

The extraction yields of the studied samples are in the order of LH10, JH2, H317, and J1 regardless of solvents (Fig. 4a), which may be due to the soluble hydrocarbon content (S_1) of the studied sample (Table 2). According to the TOC-

normalized yield of extracts, the mature samples J1 (T_{max} 449°C) had significantly higher extractables than other samples (Fig. 4b), which may be related to that the J1 sample (T_{max} 449°C) was at the peak of hydrocarbon generation, thus a large number of kerogens were cracked into oil and bitumen (Ertas et al., 2006; Wei et al., 2014). However, a little kerogen was converted to a small amount of oil in the early maturity stage (Cao et al., 2020), so the TOC-normalized extraction yield of the JH2 sample is low. However, the TOC-normalized extraction yield of late mature shale H317 is similar to that of early mature shale JH2, which could be attributed to that some of the oil is cracked to natural gas or transported to other locations with maturation (Cao et al., 2020).

5.2 Effect of solvent extraction on the chemical structure of shales

The application of FTIR spectroscopy provides an evaluation of the aromaticity and length of aliphatic chains for original shales and residues from extractions. Table 4 showed that the aromaticity (AR2 and AR3) of original shale OM with different maturity is obviously different ranging from 2.828 to 3.327. Fig. 7 shows there is a positive correlation between aromaticity and maturity in shale (Feng et al., 2013). Thus, the above-mentioned facts indicate that the thermal maturation can increase the aromaticity of shale OM.

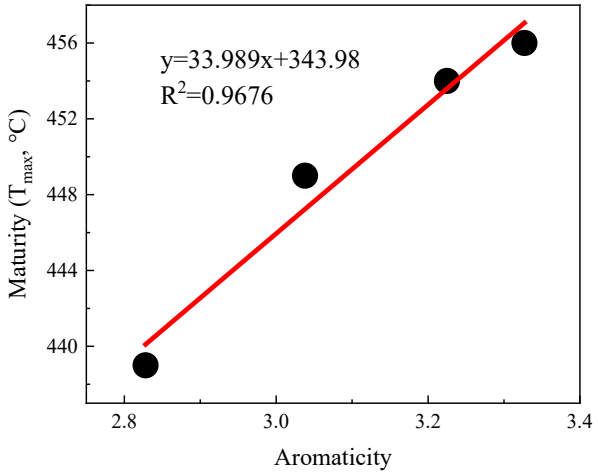

Fig. 7. Relationships between the aromaticity and the maturity in shale OM.

Table 4 showed the length of aliphatic chains (LAC) from late mature shale (i.e., LH10 and H317) is higher than those of mature shale J1 and marginally mature shale JH2. In addition, the LAC of the early mature shale J1 is also higher than the marginally mature shale JH2 (Table 4). However, the LAC of the higher mature H317 shale (T_{max}=456°C) is lower than that of mature LH10 shale (T_{max}=454°C). Those indicate that the aliphatic chains lengthened with the increase of maturity before the late maturity stage (Feng et al., 2013), and then shortened as the maturity further increases. That may be attributed to the fact that kerogen cracking to form a large amount of bitumen at the low maturity stage leads to longer aliphatic chains with increasing maturity, while at the high maturity stage bitumen is largely consumed, the OM represented by bitumen is further

cracked, thus shortening the aliphatic chains with increasing maturity (Feng et al., 2013). However, previous studies have also observed that aliphatic chains lengthened become monotonically shorter and/or more branched with maturity, which indicates that longer aliphatic chains can be preferentially cleaved. The cleavage of the C−C bonds between carbons α and β to a ring could explain this result (Lin and Ritz, 1993). Moreover, the large differences in the sources of OM in different regions may be the cause of the above contradictions.

The DOS of aromatic rings represents the fraction of aromatic sites where hydrogen atoms are substituted by alkyl groups, there is no regularity in the DOS (i.e., the fraction of aromatic sites where hydrogen atoms are substituted by alkyl groups) of different maturity shales (Table 4), therefore the fraction of aromatic sites where hydrogen atoms are substituted by alkyl groups in shale is independent of maturity.

In addition, the FTIR-derived LAC values smaller than1 show the superiority of CH_3 bands (i.e., asymmetric stretching vibration) in shales corresponding to short and branched aliphatic chains (Furmann et al., 2013). Our results demonstrate that aliphatic chains are shorter with higher branched in the original shale samples, which could not be changed during the extractions (Table 4). In addition, the FTIR of shales after different solvent extractions is irregular, which may be influenced by the inorganic minerals. Therefore, it seems much more reasonable to conclude that FTIR was unable to detect any significant change in the LAC values due to solvent extraction. Furthermore, the aromaticity (both AR2 and AR3) of residues after THF extractions is significantly higher than those after other solvents extraction (Table 4), which may be related to that THF only dissolves relatively fewer aromatic hydrocarbons from shales (Cao et al., 2020) and the residual abundant aromatic hydrocarbons in shale benefits OM aromaticity (Monger, 1984).

6 Conclusions

Soxhlet-extractions with THF, benzene, CS_2, and acetone respectively have been applied to the shale samples with a progressive maturation gradient in order to gain insights into the proportion of soluble hydrocarbon and the chemical characteristics of shale with different maturity. The following conclusions have been obtained:

1 The extraction yield of shale with THF is significantly higher than that of other solvents, which may be related to the properties of the THF, including the aromatic structure, high boiling point, excellent Hansen solubility parameters, and strong polarity. The TOC-normalized yield of the mature sample J1 is significantly higher than that of other samples, which may be related to that the J1 sample is at the peak of hydrocarbon generation, thus a large number of kerogens were cracked into oil and bitumen.

2 Thermal maturation of shales can increase the aromaticity of OM. The aliphatic chains in the shale OM lengthened with the increase of maturity before late maturity stage, and then shortened with the further increase of maturity in late maturity stage.

3 The extraction of shales with solvents hardly changes the length of aliphatic chains. Higher aromaticity is observed in shale residues after THF extractions than other solvents (i.e., acetone, CS_2, benzene).

Data availability. Data will be made available on request.

Author contributions. Yan Cao was responsible for the conceptualization and methodology of the study, carrying out the experiments, compilation and analysis of data, and writing the paper. Zhijun Jin was responsible for the acquisition and management of financial support, contribution to experimental design. Rukai Zhu and Kouqi Liu investigated and revised the ideas of the article. All authors contributed to the review of the manuscript.

Competing interests. The contact author has declared that none of the authors has any competing interests.

Disclaimer. Publisher's note: Copernicus Publications remains neutral with regard to jurisdictional claims in published maps and institutional affiliations.

Acknowledgments. This study was jointly funded by the National Science Foundation of China (42090025) and the 2022 American Association of Petroleum Geologists Foundation Grants-in-Aid Program (Grants-in-Aid General Fund Grant).

References

Abourriche, A. K., Oumam, M., Hannache, H., Birot, M., Abouliatim, Y., Benhammou, A., El Hafiane, Y., Abourriche, A. M., Pailler, R., and Naslain, R.: Comparative studies on the yield and quality of oils extracted from Moroccan oil shale, J. Supercrit. Fluids, 84, 98–104, https://doi.org/10.1016/j.supflu.2013.09.018, 2013.

Allawzi, M., Al-Otoom, A., Allaboun, H., Ajlouni, A., and Al Nseirat, F.: CO2 supercritical fluid extraction of Jordanian oil shale utilizing different co-solvents, Fuel Process. Technol., 92, 2016–2023, https://doi.org/10.1016/j.fuproc.2011.06.001, 2011.

Cao, Y., Han, H., Liu, H. wu, Jia, J. chao, Zhang, W., Liu, P. wei, Ding, Z. gang, Chen, S. jia, Lu, J. gang, and Gao, Y.: Influence of solvents on pore structure and methane adsorption capacity of lacustrine shales: An example from a Chang 7 shale sample in the Ordos Basin, China, J. Pet. Sci. Eng., 178, 419–428, https://doi.org/10.1016/j.petrol.2019.03.052, 2019.

Cao, Y., Han, H., Guo, C., Pang, P., Ding, Z. gang, and Gao, Y.: Influence of extractable organic matters on pore structure and its evolution of Chang 7 member shales in the Ordos Basin, China: Implications from extractions using various solvents, J. Nat. Gas Sci. Eng., 79, 103370, https://doi.org/10.1016/j.jngse.2020.103370, 2020.

Chen, Y., Mastalerz, M., and Schimmelmann, A.: Characterization of chemical functional groups in macerals across different coal ranks via micro-FTIR spectroscopy, Int. J. Coal Geol., 104, 22–33, https://doi.org/10.1016/j.coal.2012.09.001, 2012.

Drobniak, A. and Mastalerz, M.: Chemical evolution of Miocene wood: Example from the Belchatow brown coal deposit, central Poland, Int. J. Coal Geol., 66, 157–178, https://doi.org/10.1016/j.coal.2005.06.004, 2006.

Duan, Y., Wang, C. Y., Zheng, C. Y., Wu, B. X., and Zheng, G. D.: Geochemical study of crude oils from the Xifeng oilfield of the Ordos basin, China, J. Asian Earth Sci., 31, 341–356, https://doi.org/10.1016/j.jseaes.2007.05.003, 2008.

Ertas, D., Kelemen, S. R., and Halsey, T. C.: Petroleum expulsion part 1. Theory of kerogen swelling in multicomponent solvents, Energy and Fuels, 20, 295–300, https://doi.org/10.1021/ef058024k, 2006.

Espitalie, J., Deroo, G., and Marquis, F.: Rock-Eval pyrolysis and its applications (part 2), Rev. Inst. Fr. Pet., 40, 755–784, https://ogst.ifpenergiesnouvelles.fr/articles/ogst/abs/1985/06/vol40n6p755/vol40n6p755.html, 1985.

Feng, Y., Le Doan, T. Van, and Pomerantz, A. E.: The chemical composition of bitumen in pyrolyzed green river oil shale: Characterization by 13C NMR spectroscopy, Energy and Fuels, 27, 7314–7323, https://doi.org/10.1021/ef4016685, 2013.

Furmann, A., Mastalerz, M., Brassell, S. C., Schimmelmann, A., and Picardal, F.: Extractability of biomarkers from high- and low-vitrinite coals and its effect on the porosity of coal, Int. J. Coal Geol., 107, 141–151, https://doi.org/10.1016/j.coal.2012.09.010, 2013.

Gorynski, K. E., Tobey, M. H., Enriquez, D. A., Smagala, T. M., Dreger, J. L., and Newhart, R. E.: Quantification and characterization of hydrocarbon-filled porosity in oil-rich shales using integrated thermal extraction, pyrolysis, and solvent extraction, Am. Assoc. Pet. Geol. Bull., 103, 723–744, https://doi.org/10.1306/08161817214, 2019.

Guan, X. H., Liu, Y., Wang, D., Wang, Q., Chi, M. S., Liu, S., and Liu, C. G.: Three-Dimensional Structure of a Huadian Oil Shale Kerogen Model: An Experimental and Theoretical Study, Energy and Fuels, 29, 4122–4136, https://doi.org/10.1021/ef502759q, 2015.

Guo, H., Jia, W., Peng, P., Lei, Y., Luo, X., Cheng, M., Wang, X., Zhang, L., and Jiang, C.: The composition and its impact on the methane sorption of lacustrine shales from the Upper Triassic Yanchang Formation, Ordos Basin, China, Mar. Pet. Geol., 57, 509–520, https://doi.org/10.1016/j.marpetgeo.2014.05.010, 2014.

Hu, H., Zhang, J., Guo, S., and Chen, G.: Extraction of Huadian oil shale with water in sub- and supercritical states, Fuel, 78, 645–651, https://doi.org/10.1016/S0016-2361(98)00199-9, 1999.

Hu, S., Zhao, W., Hou, L., Yang, Z., Zhu, R., Wu, S., Bai, B., and Jin, X.: Development potential and technical strategy of continental shale oil in China, Pet. Explor. Dev., 47, 877–887, https://doi.org/10.1016/S1876-3804(20)60103-3, 2020.

Ji, L. ming, Yan, K., Meng, F. wei, and Zhao, M.: The oleaginous Botryococcus from the Triassic Yanchang Formation in Ordos Basin, Northwestern China: Morphology and its paleoenvironmental significance, J. Asian Earth Sci., 38, 175–185, https://doi.org/10.1016/j.jseaes.2009.12.010, 2010.

Johnson, R. N., Farnham, A. G., Clendinning, R. A., Hale, W. F., and Merriam, C. N.: Poly(aryl ethers) by nucleophilic aromatic substitution. I. Synthesis and properties, J. Polym. Sci. Part A-1 Polym. Chem., 5, 2375–2398, https://doi.org/10.1002/pol.1967.150050916, 1967.

Lei, Y., Luo, X., Wang, X., Zhang, L., Jiang, C., Yang, W., Yu, Y., Cheng, M., and Zhang, L.: Characteristics of silty laminae in Zhangjiatan shale of southeastern Ordos Basin, China: Implications for shale gas formation, Am. Assoc. Pet. Geol. Bull., 99, 661–687, https://doi.org/10.1306/09301414059, 2015.

Lei, Q., Weng, D., Xiong, S., Liu, H., Guan, B., Deng, Q., Yan, X., Liang, H., and Ma, Z.: Progress and development directions of shale oil reservoir stimulation technology of China National Petroleum Corporation, Pet. Explor. Dev., 48, 1198–1207, https://doi.org/10.1016/S1876-3804(21)60102-7, 2021.

Li, Y., Chen, S., Wang, Y., Su, K., He, Q., Qiu, W., and Xiao, Z.: Relationships between hydrocarbon evolution and the geochemistry of solid bitumen in the Guanwushan Formation, NW Sichuan Basin, Mar. Pet. Geol., 111, 116–134, https://doi.org/10.1016/j.marpetgeo.2019.08.018, 2020.

Li, Y., Lu, J., Liu, X., Wang, J., Ma, W., He, X., Mou, F., and Li, X.: Geochemistry and origins of natural gas in the Hong-Che fault zone of the Junggar Basin, NW China, J. Pet. Sci. Eng., 214, 110501, https://doi.org/10.1016/j.petrol.2022.110501, 2022.

Lin, R. and Patrick Ritz, G.: Studying individual macerals using i.r. microspectrometry, and implications on oil versus gas/condensate proneness and "low-rank" generation, Org. Geochem., 20, 695–706, https://doi.org/10.1016/0146-6380(93)90055-G, 1993.

Monger, T. G.: The impact of oil aromaticity on carbon dioxide flooding, Soc. Pet. Eng., https://www.osti.gov/biblio/6869910, 1984.

Lu, J., Liao, J., Liu, X., Li, Y., Yao, J., He, Q., Xiao, Z., He, X., Fu, X., and Li, X.: Geochemistry of different source rocks and oil-source correlation of lacustrine sedimentary successions: A case study of the Triassic Yanchang formation in the Dingbian-Wuqi Area, Ordos Basin, Northern China, J. Asian Earth Sci., 232, 105216, https://doi.org/10.1016/j.jseaes.2022.105216, 2022.

Masaki, K., Yoshida, T., Li, C., Takanohashi, T., and Saito, I.: The effects of pretreatment and the addition of polar compounds on the production of "HyperCoal" from subbituminous coals, Energy and Fuels, 18, 995–1000, https://doi.org/10.1021/ef049970o, 2004.

Mastalerz, M., Schimmelmann, A., Lis, G. P., Drobniak, A., and Stankiewicz, A.: Influence of maceral composition on geochemical characteristics of immature shale kerogen: Insight from density fraction analysis, Int. J. Coal Geol., 103, 60–69, https://doi.org/10.1016/j.coal.2012.07.011, 2012.

Olukcu, N., Yanik, J., Saglam, M., Yuksel, M., and Karaduman, M.: Solvent effect on the extraction of Beypazari oil shale, Energy and Fuels, 13, 895–902, https://doi.org/10.1021/ef9802678, 1999.

Overland, I.: Future Petroleum Geopolitics: Consequences of Climate Policy and Unconventional Oil and Gas, Handb. Clean Energy Syst., 1–29, https://doi.org/10.1002/9781118991978.hces203, 2015.

Peters, K. E.: Guidelines for Evaluating Petroleum Source Rock Using Programmed Pyrolysis., Am. Assoc. Pet. Geol. Bull., 70, 318–329, https://doi.org/10.1306/94885688-1704-11d7-8645000102c1865d, 1986.

Qi, Y., Ju, Y., Cai, J., Gao, Y., Zhu, H., Hunag, C., Wu, J., Meng, S., and Chen, W.: The effects of solvent extraction on nanoporosity of marine-continental coal and mudstone, Fuel, 235, 72–84, https://doi.org/10.1016/j.fuel.2018.07.083, 2019.

Qiu, X., Liu, C., Mao, G., Deng, Y., Wang, F., and Wang, J.: Late Triassic tuff intervals in the Ordos basin, Central China: Their depositional, petrographic, geochemical characteristics and regional implications, J. Asian Earth Sci., 80, 148–160, https://doi.org/10.1016/j.jseaes.2013.11.004, 2014.

Schuler, B., Meyer, G., Peña, D., Mullins, O. C., and Gross, L.: Unraveling the Molecular Structures of Asphaltenes by Atomic Force Microscopy, J. Am. Chem. Soc., 137, 9870–9876, https://doi.org/10.1021/jacs.5b04056, 2015.

Schuler, B., Fatayer, S., Meyer, G., Rogel, E., Moir, M., Zhang, Y., Harper, M. R., Pomerantz, A. E., Bake, K. D., Witt, M., Peña, D., Kushnerick, J. D., Mullins, O. C., Ovalles, C., Van Den Berg, F. G. A., and Gross, L.: Heavy Oil Based Mixtures of Different Origins and Treatments Studied by Atomic Force Microscopy, Energy and Fuels, 31, 6856–6861, https://doi.org/10.1021/acs.energyfuels.7b00805, 2017.

Shaohui, G., Shuyuan, L., and Kuangzong, Q.: CS2/NMP extraction of immature source rock concentrates, Org. Geochem., 31, 1783–1795, https://doi.org/10.1016/S0146-6380(00)00126-1, 2000.

The Oil and Gas Industry Standards of the People's Republic of China SY/T 5735–1995, Geochemical evaluation method of continental hydrocarbon source rocks, https://max.book118.com/html/2019/0831/5032240204002122.shtm, 1995.

Tong, J., Han, X., Wang, S., and Jiang, X.: Evaluation of structural characteristics of huadian oil shale kerogen using direct techniques (Solid-state 13C NMR, XPS, FT-IR, and XRD), Energy and Fuels, 25, 4006–4013, https://doi.org/10.1021/ef200738p, 2011.

Toolan, D. T. W., Isakova, A., Hodgkinson, R., Reeves-Mclaren, N., Hammond, O. S., Edler, K. J., Briscoe, W. H., Arnold, T., Gough, T., Topham, P. D., and Howse, J. R.: Insights into the influence of solvent polarity on the crystallization of poly(ethylene oxide) spin-coated thin films via in situ grazing incidence wide-angle X-ray scattering, Macromolecules, 49, 4579–4586, https://doi.org/10.1021/acs.macromol.6b00312, 2016.

Wang, Y., Liu, L., and Cheng, H.: Pore structure of Triassic Yanchang mudstone, Ordos Basin: Insights into the impact of solvent extraction on porosity in lacustrine mudstone within the oil window, J. Pet. Sci. Eng., 195, 107944, https://doi.org/10.1016/j.petrol.2020.107944, 2020.

Wang, Q., Ye, J. Bin, Yang, H. Y., and Liu, Q.: Chemical Composition and Structural Characteristics of Oil Shales and Their Kerogens Using Fourier Transform Infrared (FTIR) Spectroscopy and Solid-State 13C Nuclear Magnetic Resonance (NMR), Energy and Fuels, 30, 6271–6280, https://doi.org/10.1021/acs.energyfuels.6b00770, 2016.

Wang, Q., Hou, Y., Wu, W., Niu, M., Ren, S., and Liu, Z.: The relationship between the humic degree of oil shale kerogens and their structural characteristics, Fuel, 209, 35–42, https://doi.org/10.1016/j.fuel.2017.07.077, 2017.

Wei, L., Mastalerz, M., Schimmelmann, A., and Chen, Y.: Influence of Soxhlet-extractable bitumen and oil on porosity in thermally maturing organic-rich shales, Int. J. Coal Geol., 132, 38–50, https://doi.org/10.1016/j.coal.2014.08.003, 2014.

Yang, H., Zhou, P., Xiong, C., Yu, S., and Li, J.: Integrity Evaluation of Cement Ring during Fracturing and Flowback of Horizontal Well in Jimsar Shale Oil, Lithosphere, 2021, 1–11, https://doi.org/10.2113/2021/6519109, 2021a.

Yang, S., Qiao, H., Cheng, B., and Hu, Q.: Solvent extraction efficiency of an Eocene-aged organic-rich lacustrine shale, Mar. Pet. Geol., 126, 104941, https://doi.org/10.1016/j.marpetgeo.2021.104941, 2021b.

Yang, Z., Zou, C. N., Wu, S. T., Lin, S. H., Pan, S. Q., Niu, X. B., Men, G. T., Tang, Z. X., Li, G. H., Zhao, J. H., and Jia, X. Y.: Formation, distribution and resource potential of the “sweet areas (sections)” of continental shale oil in China, Mar. Pet. Geol., 102, 48–60, https://doi.org/10.1016/j.marpetgeo.2018.11.049, 2019.

Zhao, X., Liu, Z., Lu, Z., Shi, L., and Liu, Q.: A study on average molecular structure of eight oil shale organic matters and radical information during pyrolysis, Fuel, 219, 399–405, https://doi.org/10.1016/j.fuel.2018.01.046, 2018.

Zhou, S., Yan, D., Tang, J., and Pan, Z.: Abrupt change of pore system in lacustrine shales at oil- and gas-maturity during catagenesis, Int. J. Coal Geol., 228, 103557, https://doi.org/10.1016/j.coal.2020.103557, 2020a.

Zhou, L., Zhao, X., Chai, G., Jiang, W., Pu, X., Wang, X., Han, W., Guan, Q., Feng, J., and Liu, X.: Key exploration & development technologies and engineering practice of continental shale oil: A case study of Member 2 of Paleogene Kongdian Formation in Cangdong Sag, Bohai Bay Basin, East China, Pet. Explor. Dev., 47, 1138–1146, https://doi.org/10.1016/S1876-3804(20)60124-0, 2020b.